Human Molecular Genetics, 2014, Vol. 23, No. 14 **3792–3800**
doi:10.1093/hmg/ddu092
Advance Access published on February 23, 2014

A *piggyBac* insertion disrupts *Foxl2* expression that mimics BPES syndrome in mice

Fubiao Shi[1], Sheng Ding[1,4], Shimin Zhao[1], Min Han[1,2], Yuan Zhuang[1,3], Tian Xu[1,4] and Xiaohui Wu[1,*]

[1]State Key Laboratory of Genetic Engineering and National Center for International Research of Development and Disease, Institute of Developmental Biology and Molecular Medicine, Collaborative Innovation Center for Genetics and Development, School of Life Sciences, Fudan University, Shanghai 200433, China, [2]Howard Hughes Medical Institute, Department of Molecular, Cellular, Developmental Biology, University of Colorado, Boulder, CO 80309, USA, [3]Department of Immunology, Duke University Medical Center, Durham, NC 27710, USA and [4]Howard Hughes Medical Institute, Department of Genetics, Yale University School of Medicine, New Haven, CT 06536, USA

Blepharophimosis, ptosis, epicanthus inversus syndrome (BPES) is an autosomal dominant genetic disorder characterized by small palpebral fissures and other craniofacial malformations, often with (type I) but could also without (type II) premature ovarian failure. While mutations of the forkhead transcription factor *FOXL2* are associated with and likely be responsible for many BPES cases, how *FOXL2* affects craniofacial development remain to be understood. Through a large-scale *piggyBac* (*PB*) insertion mutagenesis, we have identified a mouse mutant carrying a *PB* insertion ~160 kb upstream of the transcription start site (TSS) of *Foxl2*. The insertion reduces, but not eliminates, the expression of *Foxl2*. This mutant, but not its revertant, displays BPES-like conditions such as midface hypoplasia, eyelid abnormalities and female subfertility. Further analysis indicates that the mutation does not affect mandible, but causes premature fusion of the premaxilla–maxilla suture, smaller premaxilla and malformed maxilla during midface development. We further identified an evolutionarily conserved fragment near the insertion site and observed enhancer activity of this element in tissue culture cells. Analyses using DNase I hypersensitivity assay and chromosome conformation capture assay in developing maxillary and periocular tissues suggest that the DNA region near the insertion site likely interacts with *Foxl2* TSS. Therefore, this mutant presents an excellent animal model for mechanistic study of BPES and regulation of *Foxl2*.

INTRODUCTION

Blepharophimosis, ptosis, epicanthus inversus syndrome (BPES) is an autosomal dominant genetic disorder characterized by eyelid malformations, and in some cases also with premature ovarian failure (1). BPES patients not only develop small palpebral fissures, epicanthus inversus and telecanthus, but also manifest non-ocular facial features, such as a broad nasal bridge and a short philtrum. Human genetic studies demonstrated that the forkhead transcription factor *FOXL2* on chromosome 3q23 was mutated in BPES patients (2,3). Intragenic mutations and genomic rearrangements affecting *FOXL2* are associated with 72 and 16% of all BPES patients, respectively (4,5).

Foxl2 expresses in the ovarian follicles, the periocular mesenchyme (PM) and the brachial arches (BAs) during mouse development (2,6). In the ovarian follicles, *Foxl2* is essential for the differentiation of granulosa cells (7,8). Induced ablation of *Foxl2* in adult ovary resulted in transdifferentiation of granulosa cells into Sertoli cells (9). Consistently, deletion of the *Foxl2* suppressor *Dmrt1* in adult Sertoli cells led to feminized testes (10). In the PM, *Foxl2* transcription is negatively regulated by the Notch signaling. A gain-of-function *Notch* transgene led to agenesis of the eyelid levator muscle, while disruption of *Foxl2* resulted in absent eyelids (8,11). In the embryonic mandibular arch, *Foxl2* was repressed by mandible-specific transcription factors *Dlx5* and *Dlx6* (6,12). However, the roles that *Foxl2* plays in the maxillary development are still unknown.

Deleterious mutations of long-range regulatory elements are reported to be responsible for several genetic diseases (13,14). For example, loss of the downstream regulatory region of *PAX6* results in aniridia (15), and disruption of a distant *SHH* enhancer causes preaxial polydactyly (16,17). The goat polled intersex syndrome (PIS) has been shown to be caused by an 11.7 kb upstream deletion that affects *FoxL2* expression

*To whom correspondence should be addressed. Tel: +86 2165643718; Fax: +86 2165643770; Email: xiaohui_wu@fudan.edu.cn

(18–20). Six percent of the BPES cases are caused by mutations outside of the *FOXL2* transcription unit, also suggests the existence of long-range regulatory elements of the disease gene (4,5). In fact, genomic studies have identified three upstream fragments required for the correct expression of *FOXL2* in cultured human cells (21).

piggyBac (PB) insertion has been shown to be an effective way to generate genetic mutations for functional study (22,23). *PB* insertion often reduces but not eliminates gene expression, facilitating the identification of specific functions of genes with highly pleiotropic knockout phenotypes. We have performed a large-scale *PB* insertion mutagenesis to identify novel disease-related functions of the genome. In this study, we show that a *PB* insertion ~160 kb upstream of the transcription start site (TSS) of *Foxl2* partially disrupted the expression of *Foxl2*, resulted in BPES-like conditions such as midface hypoplasia, eyelid abnormalities and female subfertility in the homozygotes. We report our analysis of the effects of this mutation on midface development and *Foxl2* transcription.

RESULTS

Growth retardation caused by midface defects in the mutant mice

We have identified a growth retardation mutant from a large-scale insertional mutagenesis project with the *PB* transposon in mice (22,23). At birth, the body weight of both heterozygotes (*PB/+*) and homozygotes (*PB/PB*) mice is similar to their wild-type (+/+) littermates. However, *PB/PB* animals started to lose weight on postnatal Day 17 (P17) and became 38.4% lighter at the age of weaning (P21) (Fig. 1A). Most of the homozygotes (19/23) did not survive by the end of the first month of their lives, only 8.7% (2/23) grew to adulthood (Fig. 1B).

Since malocclusion is a known cause of lower body weight at weaning, we tested this possibility by following postnatal craniofacial development of *PB/PB* mice. A shortened and curved midface profile could be recognized at birth and became more prominent at the age of 3 weeks (Fig. 1D). Mutant incisors could not occlude properly after eruption and grew unrestrictedly in the oral cavity. At the age of weaning, 75% (24/32) of the mutants occupied overgrown mandibular incisors, while others had broken incisors probably due to daily gnawing. Overgrowth of the mandibular incisors became more severe in older survivors, resulted in a tusk-like appearance (Fig. 1F). In addition to malocclusion, *PB/PB* mice often developed palpebral anomalies. Among 32 homozygous animals examined, we found 27 with bilateral small palpebral fissures and one case of unilateral small palpebral fissures. Among these 27 mice, six also showed unilateral periocular hair loss, while another one lost its periocular hair on both sides (Fig. 1D). No obvious difference in malocclusion or the palpebral defects were observed between males and females (data not shown).

To quantify changes of the craniofacial structure, we measured the skulls of 2-week-old mice by microcomputerized tomography (CT). We found normal mandibles (md), but malformed premaxillae (pmx) and maxillae (mx) in *PB/PB* mice (Fig. 1H and J). Compared with that of a heterozygous individual, the premaxilla length on the basal aspect was reduced by 48.4%, while the premaxillary angle on the lateral aspect (∠npm) was increased by 24.7% in the homozygote (Fig. 1O and P). Compared with the heterozygous maxilla, homozygous maxilla has a similar total length. However, the distance from the infraorbital fissure to the first molar (mxa) was reduced by 21.0% on the basal aspect. In contrast, the distance from the first molar to the most posterior maxilla-palatine suture (mxp) was increased by 7.8% (Fig. 1O). Malformation of premaxilla and maxilla not only resulted in smaller infraorbital fissures (iof) and palatine foramina (pf), but also led to malocclusion of the incisors (Fig. 1H and J).

Craniofacial bones develop through intramembranous osteogenesis from the sutures (24,25). Rapid growth of the neighboring bones often results in an interdigitated pattern in the suture (Fig. 1K and M). To evaluate the potential role of suture development in midface malformation, we examined the premaxilla–maxilla suture on skull preparations of *PB/PB* mice at the age of 2 weeks. Unlike what we observed in wild-type and heterozygous animals, the interdigitated pattern of sutural fibers disappeared in the homozygous mutants. Instead, we observed a relatively smooth boundary indicating the fusion of this suture (Fig. 1L and N). This result suggested that fused premaxilla–maxilla suture contributed to the craniofacial abnormalities and malocclusion in *PB/PB* animals.

Midface defects were caused by the *PB* insertion

The *PB* insertion was mapped to a TTAA site in the intron of *AK087804*, an EST without long-coding sequences (Fig. 2A). To verify that mutant phenotypes were caused by the *PB* insertion, but not by unknown mutations potentially generated during the mutagenesis, we generated revertants by crossing *PB/PB* mice with a transposase line *Act-PBase*. Ubiquitously expressed *PBase* can induce precise excision of the *PB* insertion both in somatic cells and in gametes, resulted in a true revertant carrying restored wild-type alleles ($+^R$) in the following generation (22) (Fig. 2B and C). We did not detect craniofacial defects in all 11 revertant progeny, while all three non-revertant littermates still possess the anomalies (Fig. 2D and E; Supplementary Material, Fig. S1A). These results suggested that the *PB* insertion is the causative factor of mutant defects.

PB insertion partially disrupts the expression of *Foxl2*

We then carried out experiments to identify the gene of which the expression is affected by the *PB* insertion and responsible for the craniofacial phenotype. We first excluded the non-protein-coding gene *AK087804* because it does not express in the head region of the embryo, nor in the testis, the brain, the liver, or the muscle in mice of 28 days old (Supplementary Material, Fig. S2). We next evaluated the expression of protein-coding genes within ~250 kb from the *PB* insertion in embryonic facial tissues (Fig. 2A; Supplementary Material, Table S1). Compared with those of the wild type, expression of most of the genes was unaffected in *PB/PB* embryos. However, the expression of *Foxl2* was modestly but significantly reduced (Supplementary Material, Fig. S3 and Table S1).

Because the expression of *Foxl2* in specific cell types could be more prominently affected by the insertion mutation, we further analyzed the expression changes of this gene by RNA *in situ* hybridization. *Foxl2* expression could be detected in embryonic BAs and PM. In the BA1, *Foxl2* signals are prominent at the

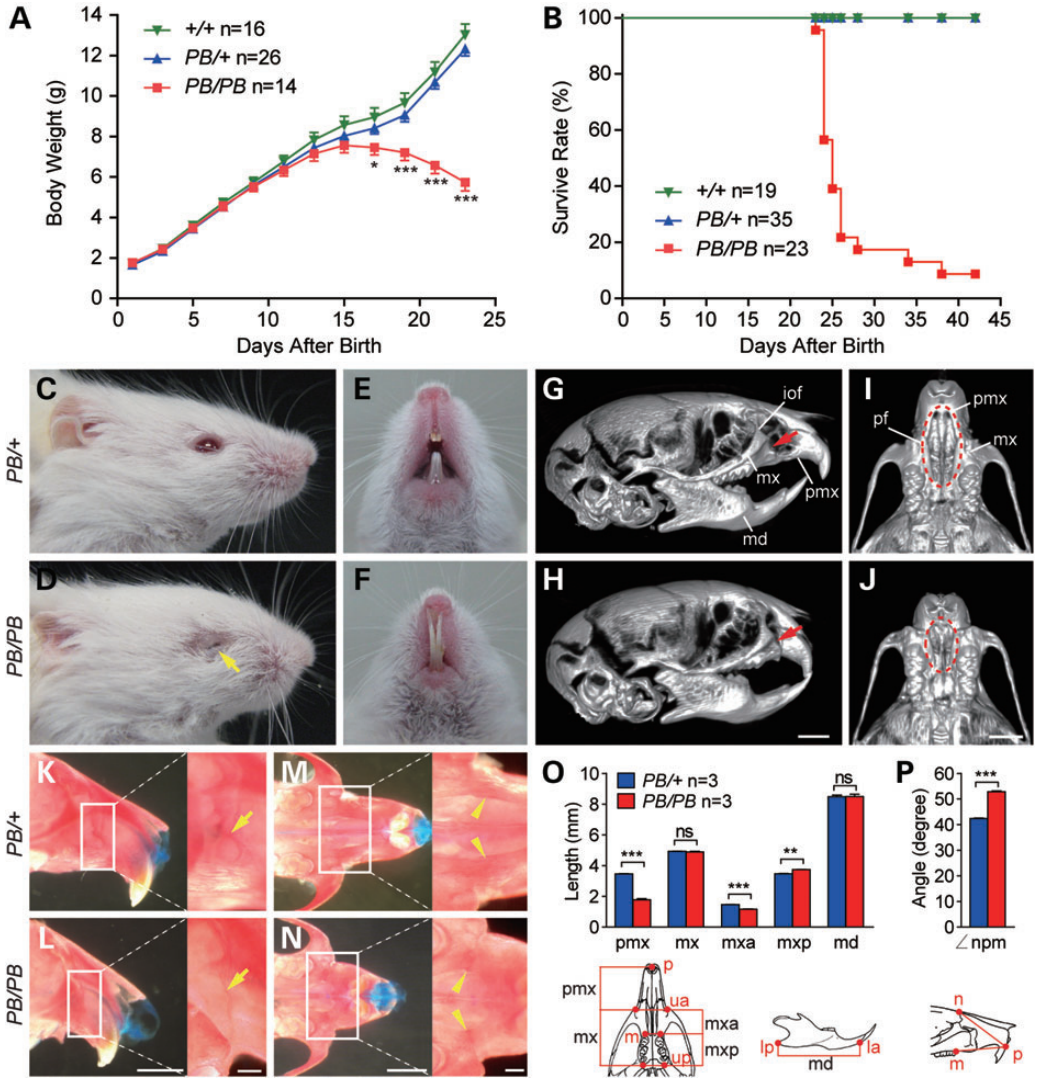

Figure 1. Growth retardation and midface defects in homozygous *PB*-insertion mutants. Growth curves showing that homozygous mutants start to lose weight on P17 (**A**) and gradually die after P23 (**B**). Representative images of the mutants at P21 (**C** and **D**) and P35 (**E** and **F**). Homozygous mice display characteristic midface profiles, small palpebral fissures (arrow, D) and overgrown lower incisors (F). (**G**–**J**) Micro-CT images of the skulls of P14 pups reveal normal mandibles (md), but malformed premaxillae (pmx) and maxillae (mx) in the homozygotes. Small infraorbital fissures (iof) (arrow, H) and short palatine foramina (pf) (circle, J) are observed in the homozygotes. (**K**–**N**) Alizarin red and Alcian blue staining of the skulls of P14 mutants. The interdigitated pattern observed in lateral (arrow, K) and ventral (arrowhead, M) views suggests a well-developed premaxillary–maxillary suture in the heterozygotes, while a smooth suture indicates premature fusion in the homozygotes (L and N). (**O** and **P**) Craniometric analysis of the P14 skulls reveals reduced anterior–posterior ratio of the maxilla (O) and larger premaxilla angle (P) in the homozygotes. The craniofacial landmarks are: n, the nasion; p, the most inferior and anterior point on alveolar process of premaxilla; m, the intersection point between the maxillary bone and the mesial surface of the upper first molar; ua, the most inferior point of the infraorbital fissure; up, the most posterior point of the maxilla-palatine suture; la, the most inferior and anterior point on alveolar process of mandible; lp, the most posterior point of angular process of mandible. Scale bars: 2 mm in (G and H), (I and J), (K and L) and (M and N); 0.5 mm in (K and L) and (M and N) insets. Data in (A), (O) and (P) represent the means ± SEM. $^{*}P < 0.05$, $^{**}P < 0.01$ and $^{***}P < 0.001$; ns, not significant.

anterior and dorsal sites of the maxillary arch (mxBA1), and weaker in the maxillary–mandibular junction at embryonic Day 10.5 (E10.5). Moderate expression of *Foxl2* could also be detected in the second BA and the third BA (BA2 and BA3, respectively) at the same stage (Fig. 3A and B). In E10.5 *PB/PB* embryos, expression of *Foxl2* became more restricted in mxBA1 (Fig. 3C), where quantification analysis revealed a 66% reduction of the *in situ* hybridization signals (Fig. 3J). Consistently, the expression of *Osr2*, a potential target of *FOXL2* (26,27), was also significantly reduced in the maxillary–mandibular junction of these embryos (Fig. 3K and L). In the PM, *Foxl2* expression is dominant at E11.5 and E12.5 (Fig. 3D, E, G and H), but significantly reduced in the *PB/PB* embryos (Fig. 3F and I). Upon the precise excision of *PB* insertion in revertant animals, *Foxl2* expression was restored to a comparable level to that of the wild-type allele (Supplementary Material, Fig. S1B and C). Taken together, these data indicated that *Foxl2* expression and function are significantly downregulated by the *PB* insertion. The mutation was therefore named as $Foxl2^{PB}$.

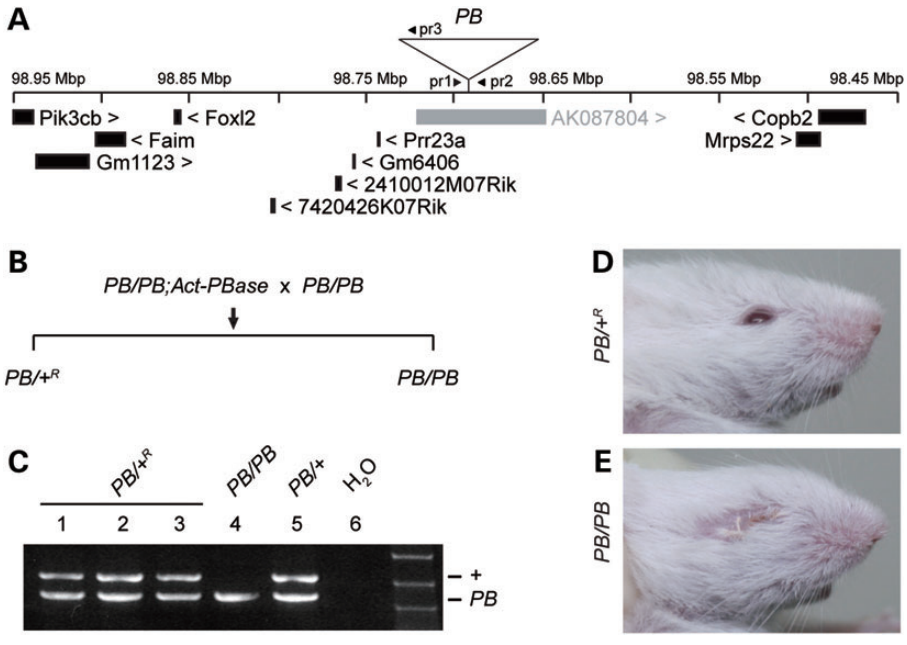

Figure 2. Verification of the causative *PB* insertion mutation. (**A**) Physical map of the 500 kb *PB* flanking sequences on mouse chromosome 9 (UCSC Genome Browser, NCBI37/mm9). Protein-coding genes are labeled as black boxes with brackets denoting the transcription direction. The *PB[Act-RFP]* element is mapped in the intron of a non-coding EST *AK087804* (gray box), with the PBR terminus close to the centromere. Arrowheads indicate the genotyping primers. (**B**) The breeding strategy to induce precise excision of the *PB* insertion. (**C**) The genotyping result of four *PBase*-negative mice (1–4 in C). Representative photographs show the craniofacial morphology of P20 revertants (**D**) and non-revertant littermates (**E**).

A long-range regulatory element of *Foxl2* near the *PB* insertion

Partial disruption of *Foxl2* expression by a distant *PB* insertion suggested the existence of long-range regulatory elements. Sequence analysis identified four evolutionarily conserved fragments (ECFs) within a 25 kb region flanking the *PB* insertion (Fig. 4A). To test whether they have transcription regulation capabilities, we generated luciferase reporters driven by a *CMV* minimal promoter in combination with individual *ECF* (Fig. 4B). We found *ECF1*, but not other three elements, could significantly enhance the expression of luciferase in 293 T cells. The luciferase activity was 25-fold more active at the presence of *ECF1* (Fig. 4C). This result suggested that *ECF1* may act as a transcription enhancer.

Long-range regulatory elements can recruit transcription factors and interact with their target promoters *in vivo* (29,30). To test whether *ECF1* was accessible to regulatory proteins during craniofacial development, we mapped the DNase I hypersensitive sites in E10.5 maxillary cells. We observed a hypersensitive subband with a probe targeting the *ECF1*-containing fragment, indicating that *ECF1* was localized in an open chromatin region (Fig. 5A and C). To further examine whether *ECF1* could interact with *Foxl2* promoter, we performed chromosome conformation capture (3C) assays with chromatin from E10.5 maxillary and E12.5 periocular cells, respectively. Specific products were amplified in both tissues with primers targeting the restriction fragments of *ECF1* and *Foxl2* TSS, respectively (Fig. 5A, D and E). These results suggested a physical interaction between *ECF1* and *Foxl2* promoter. Taken together, *ECF1* may function as a long-range enhancer of *Foxl2* during craniofacial development.

Ovarian follicle retardation and subfertility in female mutants

The craniofacial anomalies of $Foxl2^{PB/PB}$ mice are reminiscent of the conditions of BPES patients. To further explore if $Foxl2^{PB/PB}$ have the ovarian defects commonly observed in type I BPES patients, we examined the expression of *Foxl2* and the related changes in the mutant ovaries. We detected reduced ovarian expression of FOXL2 and smaller uteri and ovaries in P14 $Foxl2^{PB/PB}$ mice (Fig. 6A and C). Histological analysis showed less secondary follicles in the homozygous ovaries at this stage (Fig. 6D and E). Ovarian abnormalities persisted when $Foxl2^{PB/PB}$ females grow older. At the age of P35, while heterozygous ovaries developed antral follicles, no such follicles were observed in the homozygotes. In addition, some of the $Foxl2^{PB/PB}$ follicles occupied fewer layers of granulosa cells at this stage (Fig. 6F and G). These phenotypes may suggest retardation rather than deficiency of the ovarian follicles, since $Foxl2^{PB/PB}$ female could still produce a small number of progeny at adulthood (Fig. 6H).

DISCUSSION

We described a new allele of *Foxl2* in mice. The allele, $Foxl2^{PB}$, was generated by a *PB* insertion ~160 kb upstream from the TSS of *Foxl2*. It partially disrupted the expression of *Foxl2*, resulted in midface hypoplasia, eyelid malformation and female subfertility in homozygous animals. We also reported an evolutionary conserved element *ECF1* close to the *PB* insertion. *ECF1* may function as a long-range enhancer of *Foxl2* during craniofacial development. It not only showed transcription stimulation

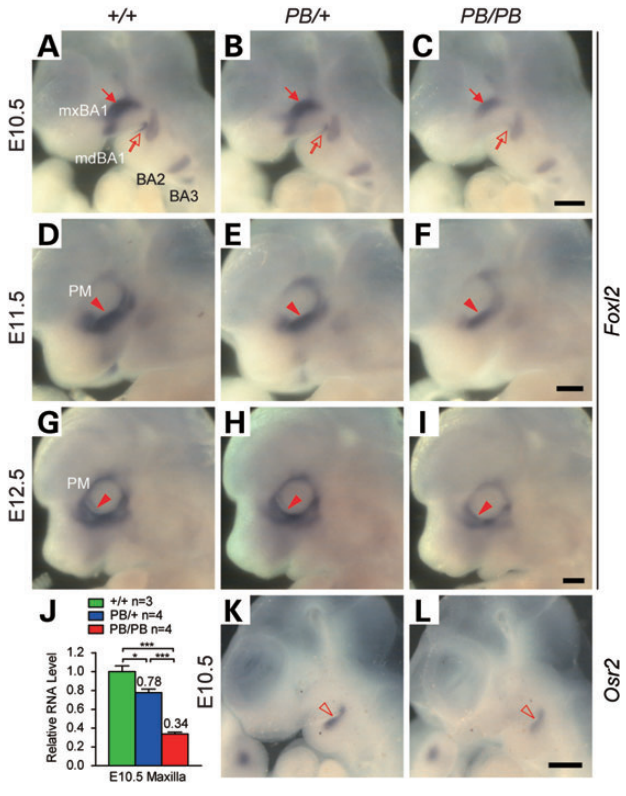

Figure 3. Reduced expression of *Foxl2* and its downstream target *Osr2* in the homozygous mutants. (**A**–**I**) *Foxl2* expression examined by whole-mount RNA *in situ* hybridization in the wild-type and mutant embryos. At E10.5, *Folx2* expression is more restricted in the maxillary arch (filled arrow) and the maxillary–mandibular junction (hollow arrow) of the homozygous embryos (C). At E11.5 and E12.5, periocular expression of *Foxl2* in the homozygotes is also weaker (filled arrowheads, F and I). (**J**) Quantification of *Foxl2* signals of mxBA1 in (A–C) reveals a 22 and a 66% reduction in *PB/+* and *PB/PB* individuals, respectively. (**K** and **L**) Expression of *Osr2*, a downstream target of *Foxl2*, is also decreased in the maxillary–mandibular junction (hollow arrowhead, L) of E10.5 *PB/PB* embryos. mxBA1 and mdBA1, the maxillary and the mandibular arch of the first branchial arch, respectively. BA2 and BA3: the second and the third branchial arch, respectively. PM, periocular mesenchyme. Scale bars: 400 μm in (A–C), (D–F), (G–I) and (K and L). Data in (J) represents means ± SEM. * $P < 0.05$; *** $P < 0.001$.

activity in tissue culture cells but also interacted with *Foxl2* promoter in the developing maxillary and periocular cells.

Foxl2 controls maxillary development in mice

The forkhead transcription factor *Foxl2* is involved in the specification of mouse gonad cells (9,10). Recently, *Foxl2* was also reported to be regulated by Notch signaling during the formation of eyelid levator smooth muscles (11). The craniofacial defects observed in $Foxl2^{PB/PB}$ mice revealed an essential role of *Foxl2* during midface skeletal development. Downregulation of *Foxl2* led to premature fusion of the premaxillary–maxillary suture, shortened premaxilla and malformed maxilla. Thus, *Foxl2* may not only contribute to the growth but also be involved in the pattern formation of the midface skeleton. The downstream targets of *Foxl2* during midface development are still unknown. Although transcriptomic analysis has suggested that the zinc finger transcription factor *OSR2* and several other factors are potential targets of *FOXL2* in human granulosa cells (26), *in situ* hybridization or real-time PCR failed to detect differential expression of these genes in the maxillary arch of homozygous animals (data not shown). Further analysis of global gene expression in specific tissues may be needed to identify targets of *FOXL2* involved in specific physiological functions.

It is interesting to note that *Foxl2* expression may be under complex spatial and temporal regulations. In $Foxl2^{PB/PB}$ embryos, *Foxl2* transcription was reduced by two-thirds in the midface progenitor tissue mxBA1 at E10.5 (Fig. 3C and J), while milder alterations were observed in other BA tissues and in the PM at different stages (Fig. 3F and I; Supplementary Material, Fig. S3). This may explain the phenotypic discrepancy between $Foxl2^{PB/PB}$ and heterozygous *Foxl2* knockout animals. In the latter case, loss of one copy *Foxl2*-coding sequence, which presumably leads to 50% reduction of the transcripts, resulted in no dramatic morphological changes in the midface (8). Alternatively or additionally, this discrepancy may reflect a difference in sensitivity to *Foxl2* expression level between these two strains with different genetic backgrounds.

$Foxl2^{PB/PB}$ mice do not display dramatic reduction in gene expression even in specific head regions, suggesting that normal development of midface is highly sensitive to the expression level of *Foxl2*. Our results may provide an explanation for that many known BPES cases are associated with mutations in the regulatory region of *FOXL2* (4,5,21). In addition, the fact that many other BPES-associated *FOXL2* mutations are likely reduction-of-function point mutations is also consistent with the idea that midface development demands full strength of *Foxl2* function (4). Therefore, our results demonstrate the value of genetic analysis using reduction-of-function mutations and *PB*-mediated mutagenesis in functional study of the genome.

ECF1 as a long-range regulatory element of *Foxl2*

Regulatory sequence mutations of *Foxl2* orthologs in different species have been previously reported. The PIS deletion reduces *FoxL2* expression from 280 kb away upstream in goat (18–20). Deletions affecting upstream genomic sequences of *FOXL2* also exist in 4% of the BPES patients (4,5). We identified an evolutionary conserved fragment *ECF1* close to the *PB* insertion in mice. Cross-species alignment of the regulatory sequences of *Foxl2* orthologs showed that *ECF1* is highly conserved among goat, mouse and human (Supplementary Material, Fig. S4A). A 3C study has detected three upstream genomic fragments interacting with *FOXL2* promoter in human KGN cells, centralizing at −177, −283 and −360 kb, respectively (21). Goat orthologs of *ECF1* and PIS deletion are close to the sequences that are conserved with the −177 and −283 kb fragments, respectively (Supplementary Material, Fig. S4B). Meanwhile, the human ortholog of *ECF1* is contained in the −177 kb fragment. Chromosome breakpoints 130, 160 or 171 kb upstream of *FOXL2* have been detected in BPES patients with balanced translocations (31–35). These translocations may isolate the transcription regulatory elements, which likely include the *hECF1*, result in misregulation of *FOXL2* in patients. We found that *ECF1* could not only stimulate transcription but also physically interact with *Foxl2* promoter in developing

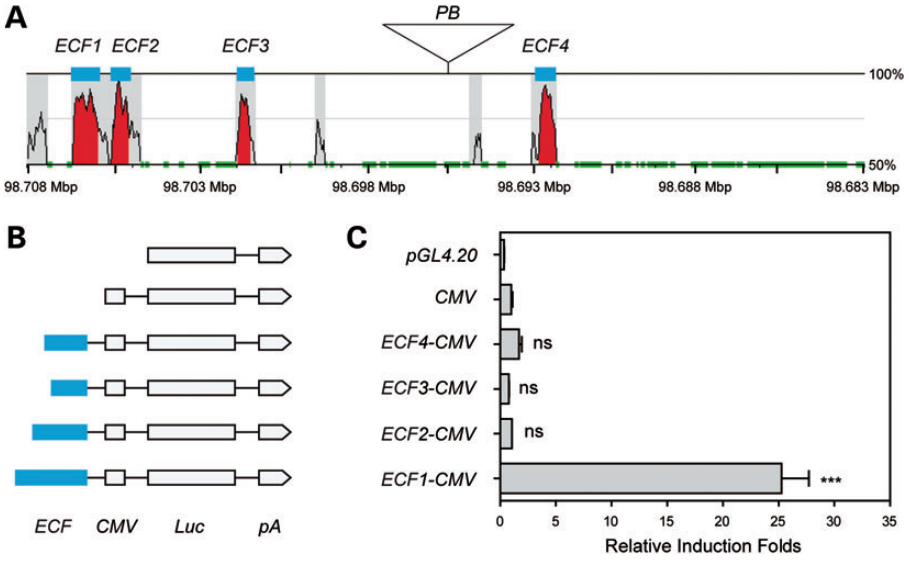

Figure 4. A conserved enhancer fragment near the *PB* insertion. (**A**) A 25 kb mouse genomic sequence flanking the *PB* insertion is aligned to its human orthologous sequence by zPicture (40). The percentage of sequence similarity is plotted based on the mouse genome. Repetitive sequences are marked in green. Fragments with opposite directions are shaded in gray. Red peaks and blue boxes indicate four *ECFs* (*ECF1–4*, length ≥200 bp and similarity ≥80%). (**B**) Luciferase reporters constructed to test the enhancer activity of individual *ECF*. *CMV*, cytomegalovirus minimal promoter; *Luc*, luciferase CDS; *pA*, SV40 polyA. (**C**) Results of luciferase reporter assay. The relative induction folds represent the means ± SEM of three experiments. $^{***}P < 0.001$; ns, not significant.

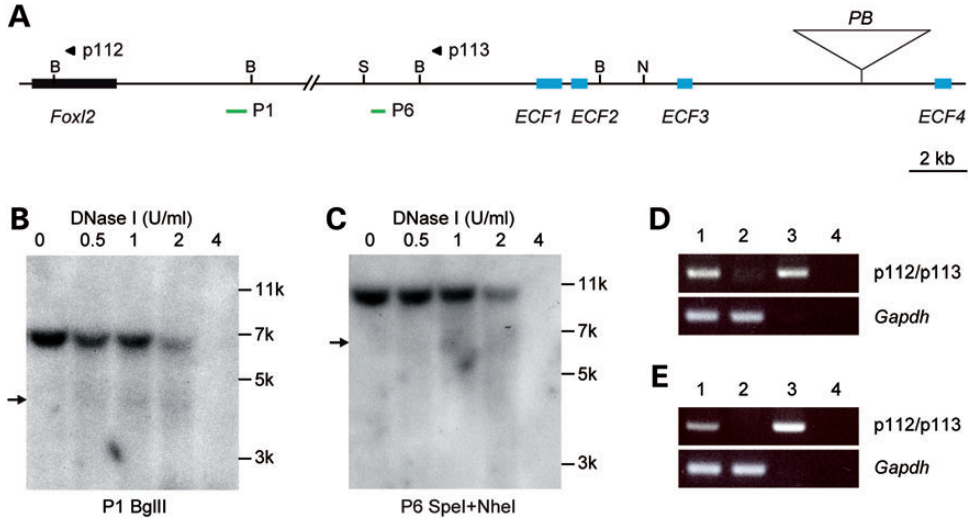

Figure 5. Chromosome confirmation analysis of *Foxl2* promoter and *ECF1*. (**A**) Restriction map of the genomic region covering *Foxl2* (black box) and the *PB* insertion. Blue boxes, *ECFs*. Green lines, probes for Southern blot. Arrowheads, PCR primers for the 3C assay. B, *Bgl*II; S, *Spe*I; N, *Nhe*I. Only the sites used to generate restriction fragments for Southern and 3C analyses are shown. (**B** and **C**) Both *Foxl2* promoter and *ECF1* are sensitive to DNase I treatment. Nuclei from E10.5 maxillary cells are harvested and treated with indicated amounts of DNase I before Southern analysis. Probe P1 is used for *Bgl*II digested DNA to detect a hypersensitive subband for the TSS of *Foxl2* (arrow, B). For *ECF1*, probe P6 is used for the blotting of *Spe*I+*Nhe*I digested DNA (C). (D–E) 3C assay of chromatin DNA from E10.5 maxillary (**D**) and E12.5 periocular (**E**) cells. PCR templates for each lanes are: 1. ligation product of *Bgl*II digested chromatin DNA; 2. *Bgl*II digested chromatin DNA without ligation; 3. *Bgl*II digested BAC DNA covering the PB and *Foxl2* region, as a positive control; 4. water. *Gapdh* is amplified as a quality control of DNA templates in Lanes 1 and 2 (lower panel).

maxillary and periocular cells. These results were consistent with the expectation that *ECF1* plays an evolutionarily conserved role in regulating *Foxl2* expression in mice, though we could not exclude the possibility that some mouse-specific genomic fragments nearby also participate in the regulation. In fact, sequence analysis does reveal that *ECF1* contains several homeodomain-binding sites (28,36) (Supplementary Material, Fig. S4A). The *PB* insertion may interfere with the interaction between *ECF1*-containing regulatory sequences and *Foxl2* promoter, or alter the high-order chromatin structure.

Foxl2$^{PB/PB}$ mice as a model of BPES

BPES patients develop eyelid abnormalities including blepharophimosis, ptosis, epicanthus inversus and telecanthus. They also manifest non-ocular features such as a broad nasal bridge

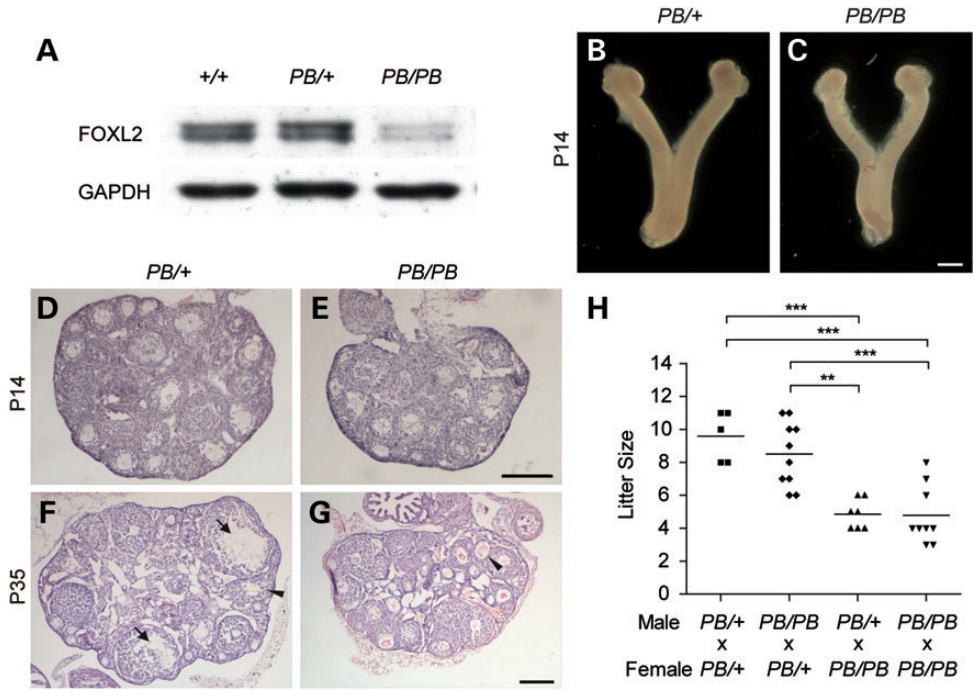

Figure 6. Ovarian follicle retardation and subfertility in female mutants. (**A**) Western blot detects lower FOXL2 expression in the ovary of P14 homozygous females. (**B** and **C**) Representative photographs show smaller uteri and ovaries of homozygous females at the same age. (**D**–**G**) Hematoxylin and eosin staining detects less secondary follicles (E) and thinner granulosa cell layers (arrowhead, G) in ovaries of P14 and P35 homozygous females. Antral follicles are present in P35 heterozygous ovaries (arrows, F) but absent in the homozygous ones. (**H**) Homozygous females produce smaller litters compared with those from heterozygous females. Pup number of each litter is plotted with the average value labeled by a horizontal bar. $^{**}P < 0.01$; $^{***}P < 0.001$; ns, not significant. Scale bars: 1 mm in (B) and (C); 100 μm in (D) and (E), (F) and (G).

and a short philtrum. *Foxl2*$^{PB/PB}$ animals exhibited comparable craniofacial defects: small palpebral fissures, shortened premaxilla and malformed maxilla. Premature ovarian failure is a typical symptom of type I BPES patients. Similarly, we observed follicle retardation and subfertility in female mutants. The fact that *Foxl2*$^{PB/PB}$ mutant recapitulated the craniofacial and ovarian conditions of type I BPES patients makes it an animal model of the disease. Quantitative description of the craniofacial defects provided here may help future in-depth characterization of human patients. This mutant may also benefit further studies of the function and transcriptional regulation of *Foxl2*.

MATERIALS AND METHODS

Mouse strains

All animal procedures were approved by the Animal Care and Use Committee of the Institute of Developmental Biology and Molecular Medicine. Both *Foxl2*^{PB} and *Act-PBase* strains were kept on the *FVB/N* background.

Histology and micro-CT

Ovaries were fixed in 4% paraformaldehyde and dehydrated in 30% sucrose before embedded in Frozen Section Medium Neg-50 (Richard-Allan Scientific). After frozen in liquid nitrogen-cooled isopentane, sections of 8 μm were prepared and stained with hematoxylin and eosin. Alizarin red and Alcian blue staining of the skeleton were performed as previously described (24).

Micro-CT data were collected by an Inveon MMCT system (SIEMENS). Craniometric analysis was performed in 3D visualization with the illustrated landmarks (Fig. 1K and L).

Reverse transcription and real-time RT-PCR

Total RNAs were extracted with Trizol (Invitrogen) and reverse transcribed (Takara), real-time PCR was performed using Brilliant QPCR Master Mix (Stratagene) following the manufacturer's instruction.

Whole-mount *in situ* hybridization

The *Foxl2* and *Osr2* cDNAs were amplified by PCR and cloned into the T-vector. RNA probes were synthesized using a DIG RNA labeling kit (Roche). Embryo whole-mount *in situ* hybridization was performed as described (37,38) and photographed with a Leica MZFLIII microscope. Hybridization signals are quantified by ImageJ (39).

Western blot

Ovary proteins were extracted in RIPA with freshly added 1 mM PMSF and 1× proteinase inhibitor (Roche). Proteins were separated on 10% SDS–PAGE. FOXL2 and GAPDH were detected by a rabbit anti-FOXL2 (1 : 1000, F0805, Sigma) and

a mouse anti-GAPDH (1 : 2000, KC-5G4, Kangcheng) antibody, respectively.

Comparative genomic analysis

A 25 kb mouse genomic sequence centralizing at the *PB* insertion (chr 9: 98 682 701–98 707 700, NCBI37/mm9) was aligned with its human ortholog (chr 3: 140 319 249–140 345 144, NCBI36/hg18) by zPicture (40). Evolutionarily conserved elements were identified under a stringent requirement of at least 80% in similarity and 200 bp in length. Cross-species alignment of the *Foxl2* upstream sequences from human (chr3: 140 145 248–140 558 578, NCBI36/hg18), mouse (chr9: 98 489 179–98 858 248, NCBI37/mm9) and goat (chr1: 127 322 877–127 806 801, CHIR1.0) were performed by mVISTA with the same stringency requirement (41).

Luciferase enhancer assay

A minimal *CMV* promoter (*pNBio*, DQ520290) was synthesized to replace the *Eco*RV–*Bgl*II fragment of *pGL4.20* to generate *CMV-Luc2*. *ECF1–4* fragments were amplified by PCR and cloned into to the *Xho*I site of *CMV-Luc2* in the same direction of *Foxl2* transcription to generate individual reporter plasmid.

293T cells were cultured in DMEM (GIBCO-BRL) with 10% fetal bovine serum at 37°C and 5% CO_2. Transfections were carried out with Lipofectamine 2000 (Invitrogen) in 24-well plates. One microgram of a reporter plasmid and 0.1 μg of the control plasmid (*pCX-nLacZ*) were applied for each well. Cells were harvested 48 h later and assayed for the luciferase and β-galactosidase activities according to standard protocols (42).

Mapping the DNase I hypersensitive sites

The maxillae from 50 E10.5 embryos were dissected and homogenized to prepare the nuclear extracts (43). Nuclear extracts equivalent to 10 embryos were digested with 0, 0.25, 0.5, 1 or 2 U DNase I (D4263, Sigma), respectively, in a total volume of 500 μl at 37°C for 5 min. The reaction was attenuated by addition of 125 μl 0.05 mM EDTA; 2.5% SDS. Genomic DNA was then purified and analyzed by Southern blot according to the standard protocol (42).

3C assay

The 3C assay were performed as described (44,45). Cross-linked chromatin DNA from 1×10^7 maxillary or periocular cells was treated with 500 U *Bgl*II (NEB) and ligated by 400 U T4 ligase (NEB). After purification, 200 ng DNA was PCR amplified for40 cycles to detect the ligation product. The BAC (RP23-9M20) containing *Foxl2* TSS and *ECF1* was used to generate randomly ligated BAC DNA for positive control template as described (45).

SUPPLEMENTARY MATERIAL

Supplementary Material is available at *HMG* online.

ACKNOWLEDGEMENTS

We thank Xiaoping Huang, Wenjun Xie and Chun Han for technical assistance, Dr Jing Zhao for the 3C protocol and Dr Wufan Tao for stimulating discussions.

Conflict of Interest statement. None declared.

FUNDING

This work was supported by the Hi-tech Research and Development Project of China (863) (2014AA021104, 2007AA022101); National Natural Science Foundation of China (NSFC) (30671109); Shanghai Rising-Star Program (06QA14006); 'Shu Guang' project of Shanghai Municipal Education Commission and Shanghai Education Development Foundation (09SG04); and the 211 and 985 projects of Chinese Ministry of Education.

REFERENCES

1. Oley, C. and Baraitser, M. (1988) Blepharophimosis, ptosis, epicanthus inversus syndrome (BPES syndrome). *J. Med. Genet.*, **25**, 47–51.
2. Crisponi, L., Deiana, M., Loi, A., Chiappe, F., Uda, M., Amati, P., Bisceglia, L., Zelante, L., Nagaraja, R., Porcu, S. *et al.* (2001) The putative forkhead transcription factor FOXL2 is mutated in blepharophimosis/ptosis/epicanthus inversus syndrome. *Nat. Genet.*, **27**, 159–166.
3. De Baere, E., Dixon, M.J., Small, K.W., Jabs, E.W., Leroy, B.P., Devriendt, K., Gillerot, Y., Mortier, G., Meire, F., Van Maldergem, L. *et al.* (2001) Spectrum of FOXL2 gene mutations in blepharophimosis-ptosis-epicanthus inversus (BPES) families demonstrates a genotype–phenotype correlation. *Hum. Mol. Genet.*, **10**, 1591–1600.
4. Beysen, D., De Paepe, A. and De Baere, E. (2009) FOXL2 mutations and genomic rearrangements in BPES. *Hum. Mutat.*, **30**, 158–169.
5. Beysen, D., Raes, J., Leroy, B.P., Lucassen, A., Yates, J.R.W., Clayton-Smith, J., Ilyina, H., Brooks, S.S., Christin-Maitre, S., Fellous, M. *et al.* (2005) Deletions involving long-range conserved nongenic sequences upstream and downstream of FOXL2 as a novel disease-causing mechanism in Blepharophimosis syndrome. *Am. J. Hum. Genet.*, **77**, 205–218.
6. Jeong, J., Li, X., McEvilly, R.J., Rosenfeld, M.G., Lufkin, T. and Rubenstein, J.L.R. (2008) Dlx genes pattern mammalian jaw primordium by regulating both lower jaw-specific and upper jaw-specific genetic programs. *Development*, **135**, 2905–2916.
7. Schmidt, D., Ovitt, C.E., Anlag, K., Fehsenfeld, S., Gredsted, L., Treier, A.C. and Treier, M. (2004) The murine winged-helix transcription factor Foxl2 is required for granulosa cell differentiation and ovary maintenance. *Development*, **131**, 933–942.
8. Uda, M., Ottolenghi, C., Deiana, M., Kimber, W., Forabosco, A., Cao, A., Schlessinger, D. and Pilia, G. (2004) Foxl2 disruption causes mouse ovarian failure by pervasive blockage of follicle development. *Hum. Mol. Genet.*, **13**, 1171–1181.
9. Uhlenhaut, N.H., Jakob, S., Anlag, K., Eisenberger, T., Sekido, R., Kress, J., Treier, A.C., Klugmann, C., Klasen, C., Holter, N.I. *et al.* (2009) Somatic Sex Reprogramming of Adult Ovaries to Testes by FOXL2 Ablation. *Cell*, **139**, 1130–1142.
10. Matson, C.K., Murphy, M.W., Sarver, A.L., Griswold, M.D., Bardwell, V.J. and Zarkower, D. (2011) DMRT1 prevents female reprogramming in the postnatal mammalian testis. *Nature*, **476**, 101–104.
11. Zhang, Y., Kao, W.W., Pelosi, E., Schlessinger, D. and Liu, C.Y. (2011) Notch gain of function in mouse periocular mesenchyme downregulates FoxL2 and impairs eyelid levator muscle formation, leading to congenital blepharophimosis. *J. Cell Sci.*, **124**, 2561–2572.
12. Depew, M.J., Lufkin, T. and Rubenstein, J.L. (2002) Specification of jaw subdivisions by Dlx genes. *Science*, **298**, 381–385.
13. Kleinjan, D.A. and van Heyningen, V. (2005) Long-range control of gene expression: Emerging mechanisms and disruption in disease. *Am. J. Hum. Genet.*, **76**, 8–32.

14. Kleinjan, D.J. and Coutinho, P. (2009) Cis-ruption mechanisms: disruption of cis-regulatory control as a cause of human genetic disease. *Brief. Funct. Genomic. Proteomic.*, **8**, 317–332.
15. Kleinjan, D.A., Seawright, A., Schedl, A., Quinlan, R.A., Danes, S. and van Heyningen, V. (2001) Aniridia-associated translocations, DNase hypersensitivity, sequence comparison and transgenic analysis redefine the functional domain of PAX6. *Hum. Mol. Genet.*, **10**, 2049–2059.
16. Lettice, L.A., Horikoshi, T., Heaney, S.J., van Baren, M.J., van der Linde, H.C., Breedveld, G.J., Joosse, M., Akarsu, N., Oostra, B.A., Endo, N. *et al.* (2002) Disruption of a long-range cis-acting regulator for Shh causes preaxial polydactyly. *Proc. Natl. Acad. Sci. USA*, **99**, 7548–7553.
17. Lettice, L.A., Heaney, S.J., Purdie, L.A., Li, L., de Beer, P., Oostra, B.A., Goode, D., Elgar, G., Hill, R.E. and de Graaff, E. (2003) A long-range Shh enhancer regulates expression in the developing limb and fin and is associated with preaxial polydactyly. *Hum. Mol. Genet.*, **12**, 1725–1735.
18. Pailhoux, E., Vigier, B., Chaffaux, S., Servel, N., Taourit, S., Furet, J.P., Fellous, M., Grosclaude, F., Cribiu, E.P., Cotinot, C. *et al.* (2001) A 11.7-kb deletion triggers intersexuality and polledness in goats. *Nat. Genet.*, **29**, 453–458.
19. Nikic, S. and Vaiman, D. (2004) Conserved patterns of gene expression in mice and goats in the vicinity of the Polled Intersex Syndrome (PIS) locus. *Chromosome Res.*, **12**, 465–474.
20. Pannetier, M., Renault, L., Jolivet, G., Cotinot, C. and Pailhoux, E. (2005) Ovarian-specific expression of a new gene regulated by the goat PIS region and transcribed by a FOXL2 bidirectional promoter. *Genomics*, **85**, 715–726.
21. D'haene, B., Attanasio, C., Beysen, D., Dostie, J., Lemire, E., Bouchard, P., Field, M., Jones, K., Lorenz, B., Menten, B. *et al.* (2009) Disease-causing 7.4 kb cis-regulatory deletion disrupting conserved non-coding sequences and their interaction with the FOXL2 promotor: implications for mutation screening. *PLoS Genet.*, **5**, e1000522.
22. Ding, S., Wu, X.H., Li, G., Han, M., Zhuang, Y. and Xu, T. (2005) Efficient transposition of the piggyBac (PB) transposon in mammalian cells and mice. *Cell*, **122**, 473–483.
23. Sun, L.V., Jin, K., Liu, Y., Yang, W., Xie, X., Ye, L., Wang, L., Zhu, L., Ding, S., Su, Y. *et al.* (2008) PBmice: an integrated database system of piggyBac (PB) insertional mutations and their characterizations in mice. *Nucleic Acids Res.*, **36**, D729–D734.
24. Kaufman, M.H. (1992) *The Atlas of Mouse Development*. Academic Press, London, UK.
25. Opperman, L.A. (2000) Cranial sutures as intramembranous bone growth sites. *Dev. Dyn.*, **219**, 472–485.
26. Batista, F., Vaiman, D., Dausset, J., Fellous, M. and Veitia, R.A. (2007) Potential targets of FOXL2, a transcription factor involved in craniofacial and follicular development, identified by transcriptomics. *Proc. Natl. Acad. Sci. USA*, **104**, 3330–3335.
27. Laissue, P., Lakhal, B., Benayoun, B.A., Dipietromaria, A., Braham, R., Elghezal, H., Philibert, P., Saad, A., Sultan, C., Fellous, M. *et al.* (2009) Functional evidence implicating FOXL2 in non-syndromic premature ovarian failure and in the regulation of the transcription factor OSR2. *J. Med. Genet.*, **46**, 455–457.
28. Laughon, A. (1991) DNA binding specificity of homeodomains. *Biochemistry*, **30**, 11357–11367.
29. Noonan, J.P. and McCallion, A.S. (2010) Genomics of long-range regulatory elements. *Annu. Rev. Genomics Hum. Genet.*, **11**, 1–23.
30. Bulger, M. and Groudine, M. (2011) Functional and mechanistic diversity of distal transcription enhancers. *Cell*, **144**, 327–339.
31. Fukushima, Y., Wakui, K., Nishida, T. and Ueoka, Y. (1991) Blepharophimosis sequence and de novo balanced autosomal translocation [46,XY,t(3;4)(q23;p15.2)]: possible assignment of the trait to 3q23. *Am. J. Med. Genet.*, **40**, 485–487.
32. Boccone, L., Meloni, A., Falchi, A.M., Usai, V. and Cao, A. (1994) Blepharophimosis, ptosis, epicanthus inversus syndrome, a new case associated with de novo balanced autosomal translocation [46,XY,t(3;7)(q23;q32)]. *Am. J. Med. Genet.*, **51**, 258–259.
33. Praphanphoj, V., Goodman, B.K., Thomas, G.H., Niel, K.M., Toomes, C., Dixon, M.J. and Geraghty, M.T. (2000) Molecular cytogenetic evaluation in a patient with a translocation (3;21) associated with blepharophimosis, ptosis, epicanthus inversus syndrome (BPES). *Genomics*, **65**, 67–69.
34. De Baere, E., Fukushima, Y., Small, K., Udar, N., Van Camp, G., Verhoeven, K., Palotie, A., De Paepe, A. and Messiaen, L. (2000) Identification of BPESC1, a novel gene disrupted by a balanced chromosomal translocation, t(3;4)(q23;p15.2), in a patient with BPES. *Genomics*, **68**, 296–304.
35. Crisponi, L., Uda, M., Deiana, M., Loi, A., Nagaraja, R., Chiappe, F., Schlessinger, D., Cao, A. and Pilia, G. (2004) FOXL2 inactivation by a translocation 171 kb away: analysis of 500 kb of chromosome 3 for candidate long-range regulatory sequences. *Genomics*, **83**, 757–764.
36. Odenwald, W.F., Garbern, J., Arnheiter, H., Tournier-Lasserve, E. and Lazzarini, R.A. (1989) The Hox-1.3 homeo box protein is a sequence-specific DNA-binding phosphoprotein. *Genes Dev.*, **3**, 158–172.
37. Correia, K.M. and Conlon, R.A. (2001) Whole-mount *in situ* hybridization to mouse embryos. *Methods*, **23**, 335–338.
38. Nagy, A. (2003) *Manipulating the Mouse Embryo: A Laboratory Manual*. Cold Spring Harbor Laboratory Press, Cold Spring Harbor, NY.
39. Abramoff, M.D., Magalhaes, P.J. and Ram, S.J. (2004) Image processing with ImageJ. *Biophotonics Int.*, **11**, 36–42.
40. Ovcharenko, I., Loots, G.G., Hardison, R.C., Miller, W. and Stubbs, L. (2004) zPicture: dynamic alignment and visualization tool for analyzing conservation profiles. *Genome Res.*, **14**, 472–477.
41. Frazer, K.A., Pachter, L., Poliakov, A., Rubin, E.M. and Dubchak, I. (2004) VISTA: computational tools for comparative genomics. *Nucleic Acids Res.*, **32**, W273–W279.
42. Sambrook, J. and Russell, D.W. (2001) *Molecular Cloning: A Laboratory Manual*. Cold Spring Harbor Laboratory Press, Cold Spring Harbor, NY.
43. Yang, T.P. and Caskey, C.T. (1987) Nuclease sensitivity of the mouse HPRT gene promoter region: differential sensitivity on the active and inactive X chromosomes. *Mol. Cell. Biol.*, **7**, 2994–2998.
44. Tolhuis, B., Palstra, R.J., Splinter, E., Grosveld, F. and de Laat, W. (2002) Looping and interaction between hypersensitive sites in the active beta-globin locus. *Mol. Cell*, **10**, 1453–1465.
45. Splinter, E., Grosveld, F. and de Laat, W. (2004) 3C technology: analyzing the spatial organization of genomic loci *in vivo*. *Methods Enzymol.*, **375**, 493–507.